

Effect of local and large-scale environments on nuclear activity and star formation

M. Argudo-Fernández^{1,2}, S. Shen^{1,3}, J. Sabater⁴, S. Duarte Puertas⁵, S. Verley^{6,7}, and X. Yang^{8,9}

¹ Key Laboratory for Research in Galaxies and Cosmology, Shanghai Astronomical Observatory, Chinese Academy of Sciences, 80 Nandan Road, Shanghai, China, 200030

² Universidad de Antofagasta, Unidad de Astronomía, Facultad Cs. Básicas, Av. U. de Antofagasta 02800, Antofagasta, Chile

³ Key Lab for Astrophysics, Shanghai, 200234, China

⁴ Institute for Astronomy, University of Edinburgh, Edinburgh EH9 3HJ, UK

⁵ Instituto de Astrofísica de Andalucía (CSIC) Apdo. 3004, 18080 Granada, Spain

⁶ Departamento de Física Teórica y del Cosmos, Universidad de Granada, 18071 Granada, Spain

⁷ Instituto Universitario Carlos I de Física Teórica y Computacional, Universidad de Granada, 18071 Granada, Spain

⁸ Center for Astronomy and Astrophysics, Shanghai Jiao Tong University, Shanghai 200240, China

⁹ IFSA Collaborative Innovation Center, Shanghai Jiao Tong University, Shanghai 200240, China

Received 2 February 2016; accepted 18 May 2016

ABSTRACT

Context. Active galactic nuclei (AGN) is one of the main drivers for transition from star-forming disk to passive spheroidal galaxies. However, the role of large-scale environment versus one-on-one interactions in triggering different types of AGN is still uncertain. We present a statistical study of the prevalence of the nuclear activity in isolated galaxies and physically bound isolated pairs.

Aims. For the purpose of this study we considered optically and radio selected nuclear activity types. We aim to assess the effect of one-on-one interaction on the fraction of AGN and the role of their large-scale environment.

Methods. To study the effect of one-on-one interaction on the fraction of AGN in isolated galaxy pairs, we compare with a sample of isolated galaxies homogeneously selected under the same isolation criterion. We examine the effect of the large-scale environment by comparing with control samples of single galaxies and galaxy pairs. To quantify the effects of local and large-scale environments we use the tidal strength parameter.

Results. In general we found no difference in the prevalence of optical AGN for the considered samples. For massive galaxies, the fraction of optical AGN in isolated galaxies is slightly higher than that in control samples. Also the fraction of passives in high mass isolated galaxies is smaller than in any other sample. Generally, there is no dependence on optical nuclear activity with local environment. On the other hand, we found evidence that radio AGN are strongly affected by the local environment.

Conclusions. Optical AGN phenomenon is related to cold gas accretion, while radio AGN is related to hot gas accretion. In this context, there is more cold gas, fuelling the central optical AGN, in isolated systems. Our results are in agreement with a scenario where cold gas accretion by secular evolution is the main driver of optical AGN, while hot gas accretion and one-on-one interactions are the main drivers of radio AGN activity.

Key words. galaxies: active – galaxies: formation – galaxies: evolution – galaxies: interactions – radio continuum: galaxies

1. Introduction

The environment in which a galaxy resides plays an important role on its formation and evolution. Galaxies suffer intrinsic and secular evolution processes (i.e. nature processes), but they are also exposed to the influences of their local and large-scale environments (i.e. nurture processes) (Casado et al. 2015). Starting from the well known morphology-density relation (Dressler 1980), other properties such as stellar mass, size, or colour are influenced by environmental processes (Peng et al. 2010; Grützbauch et al. 2011; Calvi et al. 2012; Peng et al. 2012; Boselli & Gavazzi 2014). Moreover, nuclear activity is somehow affected by galaxy environment (Kauffmann et al. 2004; Choi et al. 2009; Sabater et al. 2013).

Active galactic nuclei (AGN) also plays an important role in galaxy formation and evolution. Observations have led to the interpretation that the main driver for transition from star-forming disk to passive spheroidal galaxies is through AGN (Kauffmann et al. 2003a). A galaxy is revealed as an AGN when

its central black hole (BH) grows through mass accretion, liberating in the process a huge amount of energy (see Salpeter 1964; Lynden-Bell 1969; Soltan 1982; Fabian 1999; Alexander & Hickox 2012). There is some evidence that galaxies are more likely to host an AGN when they are interacting with a neighbour (e.g. Ellison et al. 2011). Since the most evolved and massive galaxies reside in clusters at the present day (Abell 1958; Baldry et al. 2004), the environment associated to the large-scale structure (LSS) is therefore also likely to have a significant effect on the triggering of AGN activity. However the physical processes responsible for triggering AGN, as well as the role of the environment on the fuelling of BHs, are still uncertain.

Is AGN activity connected to environment? There has been some disagreement in the literature regarding the connection between environment and nuclear activity. Differences are mainly due to sample selections and the diverse definitions of environment. The statistical studies developed by Sabater et al. (2013, 2015) suggest that large-scale environment and galaxy interactions play a fundamental but indirect role in AGN activity (by

influencing the gas supply) and that the dependence on AGN luminosity is minimal. On the other hand, the results from deep images by [Hong et al. \(2015\)](#) suggest that luminous AGN activity is associated with galaxy merging. These differences could be explained since the results of the first studies, based on Sloan Digital Sky Survey (SDSS, [York et al. 2000](#); [Strauss et al. 2002](#)) seventh data release (DR7; [Abazajian et al. 2009](#)) data, might consider merger systems as single galaxies and also be affected by the well known fibre-collision problem for close objects ([Strauss et al. 2002](#)).

Even if it can be difficult reconciling the results from one study with the results from another study, there is some consensus that secular processes may be much more important in driving the black hole growth than previously assumed ([McAlpine et al. 2015](#); [Sabater et al. 2015](#)), where the request for AGN triggering is an abundant supply of central cold gas, regardless of its origin. In the case of high luminosity AGN, major mergers appear to be the main driver ([Ellison et al. 2011](#); [Ramos Almeida et al. 2012](#); [Kaviraj et al. 2015](#); [Manzer & De Robertis 2014](#); [Satyapal et al. 2014](#); [Chiaberge et al. 2015](#)).

There are two modes of AGN activity: the 'quasar-mode' ([Shakura & Sunyaev 1973](#)), or 'cold-mode', and the 'radio-mode' ([Hine & Longair 1979](#)), or 'hot-mode'. In 'cold-mode' the AGN radiates across a broad multi-wavelength range (including optical and radio), while in 'hot-mode' AGN are mainly detectable in radio, due to the emission of their jet. The two accretion modes have different associated feedback effects in the host galaxy ([Kauffmann et al. 2003a](#); [Best et al. 2005a](#)), and they are powered by accretion of different material that can be connected to the environment ([Hardcastle et al. 2007](#); [Tasse et al. 2008](#)), but the precise origin of these differences effects remains unclear ([Best & Heckman 2012](#)).

The aim of the present study is to accurately measure the fraction of optical and radio AGN activity that is triggered by external or internal processes. With the purpose of determining the importance of secular evolution versus one-on-one interactions in triggering different types of AGN activity, we select samples of both isolated galaxies and isolated pairs. In this study we focus on isolated systems because any difference in the AGN fraction would be directly related to the addition of one companion. Also, by carefully selecting control samples of galaxy pairs and single galaxies, we go one step further and explore the effect of the large-scale environment versus one-on-one interactions on the AGN prevalence.

This study is organised as follows. In Sect. 2 we describe the samples used in this work as well as the selected AGN classification methods and the parameters used to quantify the environment. We present our results in Sect. 3 and the associated discussion in Sect. 4. Finally, a summary and the main conclusions of the study are presented in Sect. 5. Throughout the study, a cosmology with $\Omega_{\Lambda 0} = 0.7$, $\Omega_{m0} = 0.3$, and $H_0 = 70 \text{ km s}^{-1} \text{ Mpc}^{-1}$ is assumed.

2. Data and methodology

To study the effect of one-on-one interaction on the fraction of AGN, we compare isolated galaxy pairs with a sample of isolated galaxies homogeneously selected under the same isolation criterion. To understand the effect of the large-scale environment, we select control samples composed of single galaxies and galaxy pairs that can be found in any environment, from clusters or groups to voids.

2.1. Isolated galaxies and isolated pairs

We use the sample of isolated galaxies and isolated pairs compiled by [Argudo-Fernández et al. \(2015b\)](#) from the SDSS-DR10 ([Ahn et al. 2014](#)). Isolated galaxies and central galaxies in the pairs (the brightest of the pair by definition) are selected in a volume limited sample redshift range $0.005 \leq z \leq 0.080$, with $11 \leq m_r \leq 15.7$, where m_r is the SDSS model magnitude in the r -band. This criterion allows the second galaxy in the pair to be at least 2 orders of magnitude fainter within the range of spectroscopic completeness of the SDSS main galaxy sample at $m_{r,\text{Petrosian}} < 17.77 \text{ mag}$ ([Strauss et al. 2002](#)).

[Argudo-Fernández et al. \(2015b\)](#) used a three dimensional isolation criterion, based on projected distances on the sky and redshift. The systems are isolated with no neighbours in a volume of 1 Mpc projected distance within a line-of-sight velocity difference of $\Delta v \leq 500 \text{ km s}^{-1}$. After defining isolation, they followed a similar method as in [Argudo-Fernández et al. \(2014\)](#) to identify the physically bound isolated pairs. For the central galaxy in isolated pairs, [Argudo-Fernández et al. \(2015b\)](#) found an over-density of neighbours in the 2D distribution of Δv and distance d . This over-density indicates that those neighbours are likely to be physically connected. The distribution of Δv for those neighbours follows a Gaussian distribution. The neighbour galaxies within $\Delta v \leq 2\sigma$ (160 km s^{-1}) show also a tendency to be located within the first 450 kpc from the central galaxy. Conversely, neighbour galaxies at higher Δv and d would be associated to the underlying large-scale distribution of galaxies ([Argudo-Fernández et al. 2015b](#)). They found 3702 isolated galaxies, hereafter SIG (SDSS-based Isolated Galaxies), and 1240 isolated pairs physically bound at projected distances up to $d \leq 450 \text{ kpc}$ within $\Delta v \leq 160 \text{ km s}^{-1}$, hereafter SIP (SDSS-based Isolated Pairs). The SIG and SIP samples represent about 11% and 7% of the galaxies in the local Universe ($z \leq 0.080$; [Argudo-Fernández et al. 2015b](#)). The average projected distance and Δv of the SIP sample is $d \approx 215 \text{ kpc}$ and $\Delta v \approx 65 \text{ km s}^{-1}$. The average stellar mass¹ ratio in isolated pairs ($\frac{M_{\star B}}{M_{\star A}}$, where A corresponds to the central galaxy and B to the faintest galaxy in the pair) is $\frac{M_{\star B}}{M_{\star A}} \approx 0.30$, in the range $0.01 \leq \frac{M_{\star B}}{M_{\star A}} \leq 1.00$ (see [Argudo-Fernández et al. 2015b](#), for further details).

2.2. Control galaxy samples

The control samples are based on the catalogue of groups compiled by [Yang et al. \(2007\)](#), which is based on the NYU-VAGC ([Blanton et al. 2005](#)) updated with SDSS-DR7 data. [Yang et al. \(2007\)](#) developed a halo-based group finder that is optimized for grouping galaxies that reside in the same dark matter halo, including isolated galaxies in small mass haloes. Group members are complete to $M_r \leq -19.5$ absolute magnitude and $z \leq 0.090$. Nevertheless, some SDSS-DR12 ([Alam et al. 2015](#)) and LAMOST (Large Sky Area Multi-Object Fiber Spectroscopic Telescope, [Zhao et al. 2012](#)) redshifts are supplied to update the group catalogue ([Shen et al. 2016](#)).

To study the dependence of the large-scale environment on nuclear activity in galaxy pairs, we selected the central (brightest) galaxy in groups composed of two members in [Yang et al. \(2007\)](#), hereafter the SDSS pairs sample. Following the same

¹ Stellar masses in the SIG and SIP samples come from the fitting to the spectral energy distribution on the five SDSS bands using the routine `kcorrect` ([Blanton & Roweis 2007](#)) and the relation between the stellar mass-to-light ratio and color of [Bell et al. \(2003\)](#).

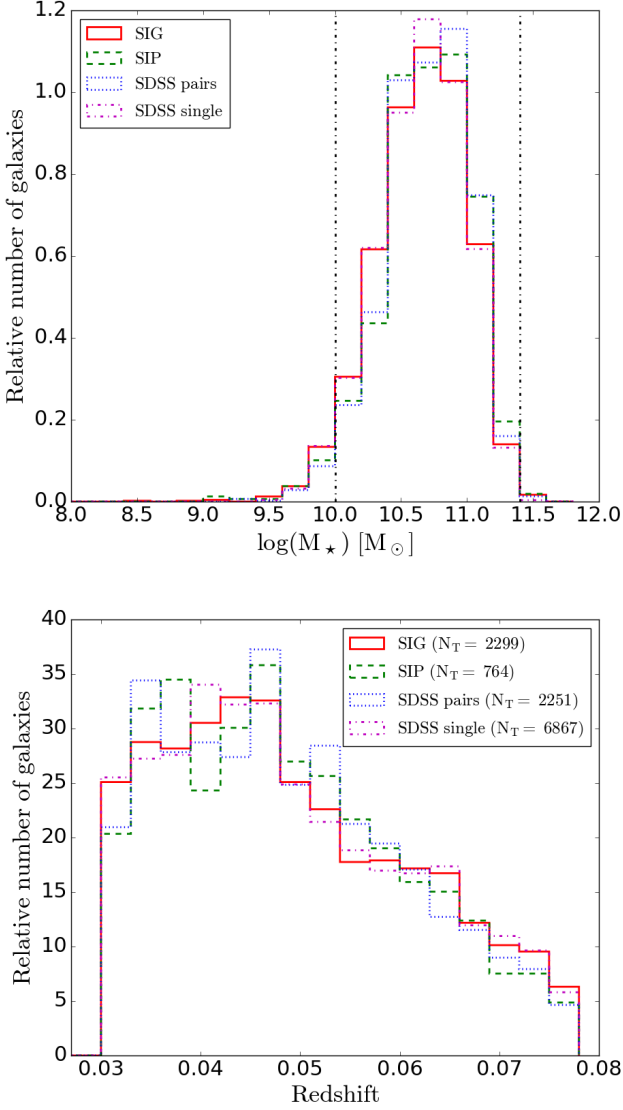


Fig. 1. *Upper panel:* Distribution of the stellar masses of the SIG and SDSS single galaxies (red solid and magenta dash-dotted histograms, respectively), and for central SIP and SDSS pairs (green dashed and blue dotted histograms, respectively). The vertical black dashed lines correspond to the selected stellar mass range for the study at $10.0 \leq \log(M_*) \leq 11.4$ [M_\odot]. *Lower panel:* Distribution of the redshift of the SIG and SDSS single galaxies (red solid and magenta dash-dotted histograms, respectively), and for central SIP and SDSS pairs (green dashed and blue dotted histograms, respectively), for galaxies within the stellar mass limited sample (N_T).

criteria, we selected one-member groups in Yang et al. (2007), hereafter the SDSS single sample, as a control sample to compare with SIG galaxies.

The average projected separation and Δv of SDSS pairs is $d \simeq 200$ kpc and $\Delta v \simeq 85$ km s $^{-1}$, similar to the SIP sample, where the 90% of the pairs show projected separations

$d \lesssim 450$ kpc and $\Delta v \lesssim 200$ km s $^{-1}$. The stellar mass² ratio also spans a similar range with an average value $\frac{M_{*B}}{M_{*A}} \simeq 0.23$.

We selected control samples within the same volume limited sample where the isolated systems were defined ($11 \leq m_r \leq 15.7$ and $0.005 \leq z \leq 0.080$) to avoid biases. We also removed the galaxies in common with the SIP or SIG catalogues. Following these criteria, the SDSS pairs sample is composed of 3772 pairs (after removing 505 pairs in common with the SIP), and the SDSS single sample is composed of 9,526 galaxies (after removing 2027 galaxies in common with the SIG).

2.3. Stellar masses and AGN classification

For the purpose of this study we considered optically and radio selected nuclear activity types. In particular, we used published stellar masses and AGN classifications for galaxies in the SDSS-DR7 from Sabater et al. (2013), hereafter SBA13 classification.

SBA13 used information about total stellar masses from Kauffmann et al. (2003b) and optical AGN classification from BPT diagnostic (Baldwin et al. 1981; Kauffmann et al. 2003a). Data based on optical spectra, i.e. the stellar masses and the corrected emission-line fluxes used to built BPT diagrams, were drawn from the Max Plank Institute for Astrophysics and Johns Hopkins University (MPIA-JHU³; Kauffmann et al. 2003b; Tremonti et al. 2004; Salim et al. 2007) added value catalogue (Brinchmann et al. 2004).

Radio AGN galaxies in SBA13 are considered if they are classified as radio AGN by Best & Heckman (2012) with a radio luminosity brighter than $L_{1.4 \text{ GHz}} \approx 10^{23} \text{ W m}^{-2} \text{ Hz}^{-1}$ (see SBA13, for more details). The radio AGN classification in Best & Heckman (2012) is based on radio-continuum data from the National Radio Astronomy Observatory (NRAO) Very Large Array (VLA) Sky Survey Condon et al. (NVSS, 1998) and the Faint Images of the Radio Sky at Twenty centimetres (FIRST, Becker et al. 1995) data bases, and follows the techniques presented in Best et al. (2005b).

Even if we take care on selecting galaxies in the control samples within the same volume limited as isolated galaxies and isolated pairs, it is well known that AGN fraction depends strongly on stellar mass (Kauffmann et al. 2003a; Peng et al. 2010, 2012). Henceforth, to have a robust control sample for the comparisons, we selected galaxies in the SDSS single and SDSS pairs samples with similar stellar mass⁴ and redshift distributions than the SIG and SIP samples, respectively (with Kolmogorov-Smirnov p-value greater than 0.80, which ensures that the distributions of the two samples are the same). To have enough numbers of objects in each mass bin for each sample, we also considered galaxies with stellar masses within the range $10.0 \leq \log(M_*) \leq 11.4$ [M_\odot] (see the upper panel in Fig. 1). The final number of galaxies, in the stellar mass range considered in this study, with available SBA13 classification is shown in the first row of Table 1.

Due to the number of galaxies in our samples, we only separate nuclear activity into optical AGN, radio AGN, star-forming

² Stellar masses in the group catalogue were computed fitting the spectral energy distribution on the five SDSS + JHK bands using the routine kcorrect (Blanton & Roweis 2007) and the relation between the stellar mass-to-light ratio and color of Bell et al. (2003) (see Yang et al. 2007, for further details).

³ Available at <http://www.mpa-garching.mpg.de/SDSS/DR7/>

⁴ Note that stellar masses from Argudo-Fernández et al. (2015b) and Yang et al. (2007) are calculated slightly different, therefore in order to use a consistent source, we consider stellar masses in SBA13.

Table 1. Number of galaxies of each type in each sample.

Type	SIP	SDSS pairs	SIG	SDSS single
Total	764	2251	2299	6867
Optical AGN	387	1009	1153	3027
LINER	152	454	482	1081
Seyfert	44	96	123	266
TO	191	459	548	1680
SFN	169	564	587	1777
Passive	208	678	559	2063
Radio AGN	10	39	11	22
HERG	1	2	0	0
LERG	8	37	11	22

Notes. Meaning of the different types: Total – total number of galaxies in each sample; Optical AGN – galaxies classified as LINER, Seyfert, or transition objects (TO); SFN – star forming nuclei galaxies; Passive – galaxies with no optical nuclear activity; Radio AGN – galaxies classified as HERG or LERG radio AGN with $L_{1.4 \text{ GHz}} \geq 10^{23} \text{ W m}^{-2} \text{ Hz}^{-1}$.

nuclei (SFN), and passive galaxies (in case that no optical nuclear activity is detected). Optical AGN classification covers transition objects (TO), Seyfert (Seyfert 1 not included), and low-ionization nuclear emission-line region (LINER; Heckman 1980) galaxies. In the case of radio AGN, this includes low-excitation (LERG) and high-excitation (HERG) radio galaxies. The number of galaxies in each sample, classified in each type and subtypes of nuclear activity, is shown in Table 1. Note that Best & Heckman (2012) classified radio galaxy into HERG and LERG when such classification was possible. Given that there is only one SIP galaxy without classification we rejected this galaxy in the present study. Besides, the three HERG galaxies present in the sample were discarded during the comparisons. Henceforth, with the term radio AGN we will be considering only LERG radio AGN.

Note that, to have a statistically significant number of galaxies, we do not impose any limit on the $[\text{O III}]_{5007}$ emission line luminosity. Some low luminosity AGN (usually LINERs) at higher redshifts could be classified as passive if their emission is not strong enough to be detected. However, the overall effect is minimized if the redshift distribution of the samples is relatively similar as it is in our case (see lower panel in Fig. 1).

Note also that AGN classification based on purely emission-line BPT diagrams are affected by uncertainties (Sabater et al. 2012). According to Rosario et al. (2016), these uncertainties are specially important for massive main-sequence local galaxies that might be misclassified as passives. We have checked that less than the 4% of the total number of galaxies in each sample in our study would be affected. Given this number, we do not expect any change in the observed trends for SFN galaxies. The results of Sabater et al. (2012) suggest that at least some of these misclassified galaxies could be classified as LINERs or Seyferts if the uncertainties were taken into account. However, given that our samples follow the same classification criteria and a relatively similar distribution in mass and redshift, the possible effect on the comparison between samples will be minimised.

2.4. Environmental parameters

Argudo-Fernández et al. (2015b) also provided the isolation degree for isolated galaxies and central galaxies in isolated pairs. They quantified the influence of both, local and large-scale envi-

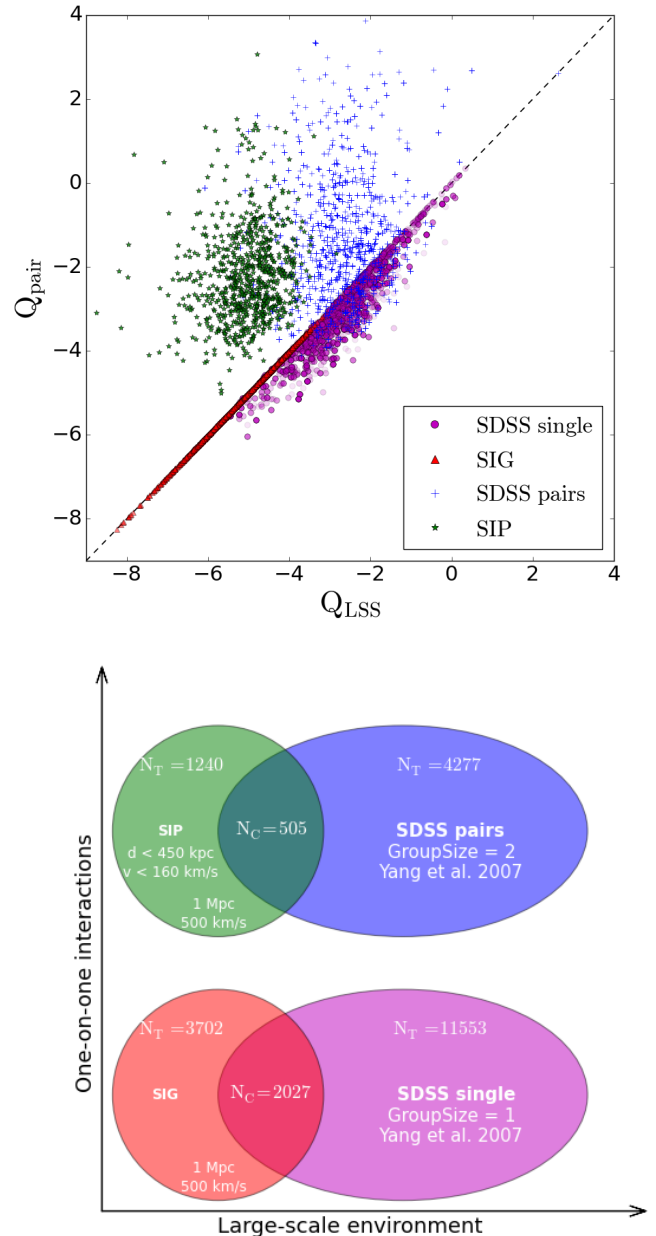


Fig. 2. Upper panel: Comparison of Q_{pair} versus Q_{LSS} , isolated pairs (green stars), SDSS single galaxies (magenta circles) and SDSS pairs (blue pluses). Note that for isolated galaxies (red triangles) there is not available Q_{pair} but we consider $Q_{\text{pair}} = Q_{\text{LSS}}$ for comparison purposes. The black dashed line represents the line where $Q_{\text{pair}} = Q_{\text{LSS}}$. Lower panel: Schema of the sample definition, total number of galaxies (N_T) in each sample and number of galaxies in common (N_C), and environment definition for the SIG and SIP samples (red and green circles, respectively), and for control samples (blue and magenta ellipses for SDSS pairs and SDSS singles respectively). The arrows in the axis indicates the direction to higher values of the tidal strength.

ronments, using the tidal strength parameter (Verley et al. 2007; Sabater et al. 2013; Argudo-Fernández et al. 2013, 2014).

To study the influence of the large-scale environment on the AGN fraction for isolated galaxies and isolated pairs, we selected the tidal strength exerted by all the galaxies in the LSS up

to 5 Mpc, Q_{LSS} (Eq. 1). For isolated pairs, we study the influence of the companion using the local tidal strength Q_{pair} (Eq. 2).

Galaxies in the LSS are defined within a volume of 5 Mpc projected distance and line-of-sight velocity difference of $\Delta v \leq 500 \text{ km s}^{-1}$. Then, for each galaxy, i , in the LSS at a projected distance $d_{LSS,i}$, the total tidal strength on the isolated galaxy (SIG), or the central (brightest) galaxy in isolated pairs (SIP), is:

$$Q_{LSS} \equiv \log \left(\sum_i \frac{M_{LSS,i}}{M} \left(\frac{D}{d_{LSS,i}} \right)^3 \right), \quad (1)$$

where M is the stellar mass and D^5 is the estimated diameter of the SIG/SIP galaxy. Stellar masses for galaxies in the LSS ($M_{LSS,i}$) were calculated by fitting the spectral energy distribution, on the five SDSS bands, using the routine kcorrect (Blanton & Roweis 2007).

We quantify the effect of the local environment as the tidal strength affecting the central (brightest) galaxy in a galaxy pair. Then, similarly to the definition of the Q_{LSS} but only considering two galaxies, the local tidal force exerted by the faintest B galaxy on the brightest (central) A galaxy is:

$$Q_{pair} \equiv \log \left(\frac{M_B}{M_A} \left(\frac{D_A}{d_{AB}} \right)^3 \right), \quad (2)$$

where d_{AB} is the projected physical distance between the galaxies of the isolated pair.

We follow the same methodology to estimate the tidal strength for control samples, i. e. we estimate Q_{LSS} for SDSS single galaxies, and Q_{pair} for SDSS pairs. A scheme of the environment for the four samples is shown in Fig. 2. For comparison purpose, Q_{pair} for SDSS single galaxies is estimated considering their first nearest neighbour. In the case of the SIG sample, as the nearest neighbour is at least at 1 Mpc away, the value of the tidal strength exerted by this neighbour is practically the same as the one exerted by the LSS, we therefore consider $Q_{pair} = Q_{LSS}$. Q_{LSS} for the control samples is estimated as for SIG and SIP, considering their LSS up to 5 Mpc. The greater the value of Q , the less isolated from external influence the galaxy. Therefore, as it is schematically shown in the lower panel of Fig. 2, the SIG and SIP samples have the same degree of isolation with respect to the LSS, while control samples extend a broader range of large-scale environments. With respect to the local environment, SIG and SDSS singles have a similar range, while the effect is stronger for central galaxies in the SIP and SDSS pairs samples. Then at fixed stellar mass, higher values of Q_{pair} are related to closer pairs. Since there is a strong dependence of AGN with stellar mass, it is recommendable to make a separated study in different stellar mass bins (SBA13).

The black dashed line in the upper panel of Fig. 2 corresponds to the line where $Q_{pair} = Q_{LSS}$. When a galaxy is located on this line, the contributions by its local and large-scale environment on the total tidal strengths are the same. Central galaxies in the SIP sample are located above the line, which means that their tidal strengths are dominated by their close environment. In fact, more than 95% of the total tidal strength in SIP galaxies is due to the companion galaxy in the pair (Argudo-Fernández et al. 2015b). In general SDSS pairs are also located above the line,

but there are some pairs below the line. These are pairs located in high density environments, mainly in clusters, surrounded by massive and nearby galaxies which are likely affecting their evolution.

3. Results

3.1. AGN prevalence

We aim to study the prevalence of AGN in the four samples previously selected. To do this we compare the relative fraction of each type of AGN in isolated galaxies and in physically bound isolated pairs, with respect to the ones found in the control samples. Due to the strong dependence of the prevalence of AGN with mass of the host galaxy, both in optical (Kauffmann et al. 2003a) and radio (Best et al. 2005a), we fix a stellar mass range in each step of the study. We considered galaxies in each sample with stellar masses within $10.0 \leq \log(M_\star) \leq 11.4 [M_\odot]$, as explained in Sect. 2, and we divided our studies in different stellar mass bins.

3.1.1. Optical AGN

The relative fraction of optical nuclear activity (SFN, optical AGN, and passive galaxies) for each sample is shown in the upper panels in Fig. 3. We considered seven stellar mass bins to observe the possible trends for each sample. Note that we take care of having a significant number of galaxies in each bin. Error bars are given by considering binomial distribution⁶.

The fraction of passive galaxies (right panel) increases with stellar mass, while the general trend for SFN galaxies (middle panel) is to decrease with stellar mass. The general trend for the fraction of optical AGN up to $\log(M_\star) \lesssim 11.0 [M_\odot]$ is to increase with stellar mass (left panel). We only find significant differences between samples for massive galaxies. The fraction of optical AGN is still increasing at higher masses for isolated galaxies while it starts to decrease in the remaining samples. Accordingly, the fraction of passive isolated galaxies is lower at higher masses.

Lower panels in Fig. 3 shows the relative fraction of each optical AGN type (LINER, Seyfert, and TO). When considering optical AGN subtypes, we find that the prevalence of LINER follows the general trend of passive galaxies. On the other hand, the fraction of TOs follows the general trend observed for star-forming galaxies. Again, there is a break point at $\log(M_\star) \lesssim 11.0 [M_\odot]$ where we start to observe significant differences between the samples. At high stellar masses there is a higher fraction of TOs and a lower fraction of LINERs SIP galaxies.

3.1.2. Radio AGN

Given that we have a low number of radio AGN galaxies in each sample (see last row in Table 1), we compare the activity between systems composed of one galaxy (SIP and SDSS single galaxies) and galaxy pairs (SIP and SDSS pairs). The fraction of radio AGN is shown in Fig. 4. The fraction of radio AGN increases steeply with the stellar mass. The prevalence of radio AGN in pairs is significantly higher than in single galaxies for the most massive galaxies.

⁵ $D = 2ar_{90}$, where r_{90} , the Petrosian radius containing 90 % of the total flux of the galaxy in the r -band, is scaled by a factor $\alpha = 1.43$ to recover the D_{25} (Argudo-Fernández et al. 2013).

⁶ $e_f = \sqrt{\frac{f(1-f)}{N_T}}$, where f is the relative fraction for a total number of N_T galaxies in each sample.

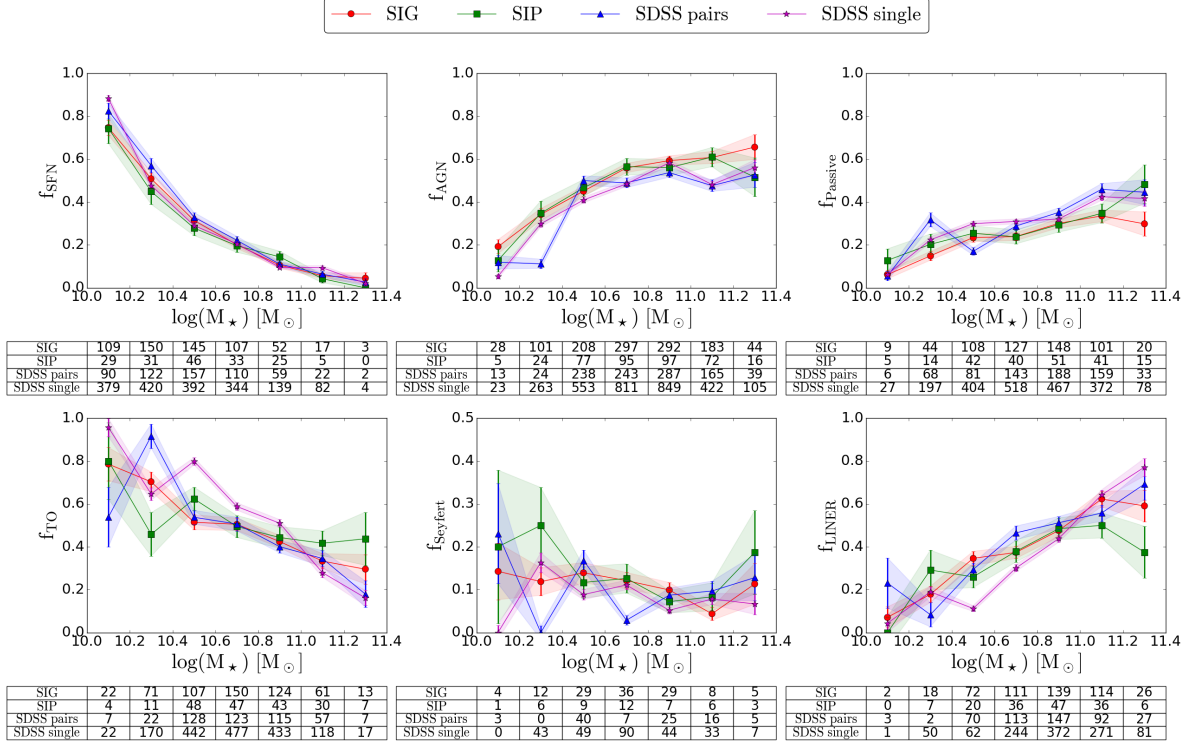


Fig. 3. *Upper panels:* Fraction of SFN (left panel), optical AGN (middle panel), and passive galaxies (right panel) with respect to stellar mass. The fraction in SIG ($N_T = 2299$) and SIP ($N_T = 764$) galaxies is depicted by red circles and green squares respectively. For the control samples, blue triangles correspond to the fraction in SDSS pairs ($N_T = 2251$) and magenta stars for SDSS single galaxies ($N_T = 6867$). The number of galaxies in each stellar mass bin is shown in tables for each sample at the bottom of each panel. Error bars are given by considering binomial distribution. *Lower panels:* Fraction of each AGN subtype with respect to stellar mass for SIG ($N_T = 1153$) and SDSS single ($N_T = 3027$) galaxies, and central galaxies in SIP ($N_T = 387$) and SDSS pairs ($N_T = 1009$). The fraction of LINER (left panel), Seyfert (middle panel), and TO (right panel) galaxies is shown in tables for each sample at the bottom of each panel.

It would be possible to lower the radio detection limit to study the radio nuclear activity for a wider range of stellar masses (Best et al. 2005a). The downside is that the closer the Universe less volume and less of each type galaxies, therefore the number of galaxies would be not statistically significant.

3.2. Influence of the environment

After studying the prevalence of optical nuclear activity as a function of mass, we investigate its relation with the local and large-scale galactic environments. We take into account the effect of the mass dividing the samples into three stellar mass bins: low-mass galaxies ($10.0 \leq \log(M_*) < 10.5$ [M_\odot]), intermediate-mass galaxies ($10.5 \leq \log(M_*) < 11.0$ [M_\odot]) and high-mass galaxies ($11.0 \leq \log(M_*) \leq 11.4$ [M_\odot]). As introduced in Sect. 2, we use Q_{pair} to quantify the influence of the companion, and Q_{LSS} to quantify the effect of the LSS. Given the low statistics for radio AGN and AGN subtypes, we perform this part of the study on the fraction of optical AGN, SFN, and passive galaxies in each sample.

3.2.1. Dependence on the local environment

According to Argudo-Fernández et al. (2014, 2015b), about 99% of the total tidal strength is due to the effect of the physically bound companions. Therefore, to investigate the dependence of nuclear activity with the local environment we restrict our study to the SIP and the SDSS pairs samples.

The fraction of nuclear activity, segregated in stellar mass bins, with respect to the Q_{pair} for central galaxy in the SIP and SDSS pairs samples, is shown in the left and right columns in the Fig. 5, respectively. Higher values of the Q_{pair} correspond to a stronger interaction between the two galaxies in the pair. In general we do not see any trend in the fraction of SFN, AGN, or passive galaxies with the local environment. Moreover, there are no significant differences between the SIP and SDSS samples in the area with common values of Q_{pair} . We further explore the dependence on the local environment and discuss these results in Sect. 4.

3.2.2. Dependence on the LSS environment

As introduced in Sect. 2, we use the Q_{LSS} to explore the effect of the large-scale environment on the fraction of nuclear activity. We do not find significant differences in the trends for the SIG and SIP samples, as well as for the control samples. Henceforth, for a clearer analysis of the results, we focus on the comparison between SIG and SDSS single galaxies to explore the effect of the large-scale environment.

Similarly to Fig. 5, Fig. 6 shows the fraction of optical nuclear activity, segregated in stellar mass bins, with respect to Q_{LSS} , in this case for the SIG and SDSS single galaxies. In general, there is no clear dependence on the large-scale environment in the nuclear activity for SDSS single galaxies. However there is a strong effect in isolated galaxies, with different trends de-

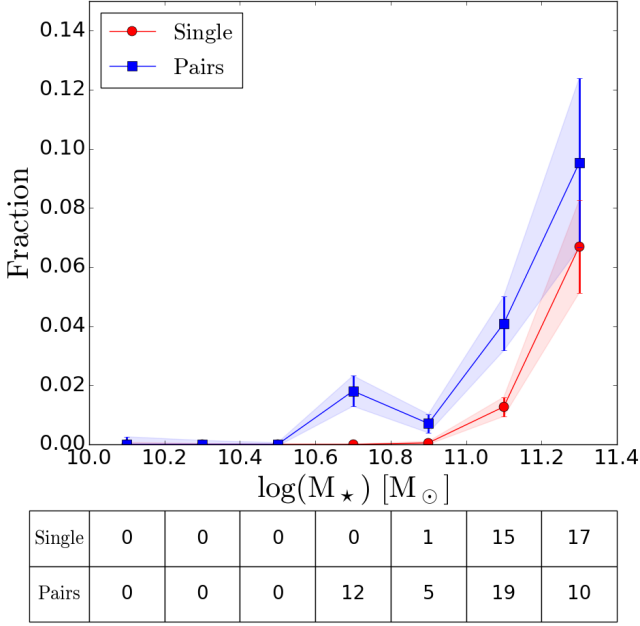


Fig. 4. Fraction of radio AGN (LERG) with respect to stellar mass. Red circles represent the join sample of SIG and SDSS single galaxies ($N_T = 33$), and blue squares represent the sample of galaxies in pairs, composed of SIP and SDSS pairs ($N_T = 45$). The number of galaxies in each stellar mass bin is shown in the table at the bottom. Error bars are given considering binomial distribution.

pending on stellar mass. We discuss these trends in more details in Sect. 4.

4. Discussion

4.1. AGN prevalence

We study the optical and radio AGN prevalence in each sample to explore the different mechanisms triggering nuclear activity. In particular, we will relate the obtained results to the different sources of gas that can fuel AGN. Depending on the nature (environment) of the studied samples, these mechanisms could be: 1) the internal and slow mass loss caused by the central BH (internal secular evolution), 2) the external and slow prolonged gas in-fall or the galaxy harassment (environmental secular evolution), or 3) the external and fast ram-pressure stripping or galaxy mergers.

4.1.1. Optical AGN

The general trend of optical AGN and passive galaxies is to increase with stellar mass, while the fraction of star forming galaxies decreases from low-mass to massive galaxies, as it is shown in the upper panels in Fig. 3. These monotonic trends with stellar mass are expected because of the ‘downsizing’ effect.

We find that, in general, there is no difference in the fraction of optical AGN for the four samples. This result points out that optical AGN is independent of the local environment, and is therefore in agreement with the general consensus that secular evolution is a main mechanism triggering optical AGN in the Local Universe (Coziol et al. 2011; Sabater et al. 2012, 2013; Hernández-Ibarra et al. 2013; Sabater et al. 2015; Pulatova et al. 2015; Hernández-Ibarra et al. 2016). As a consequence, the

prevalence of optical nuclear activity is independent to the addition of one single companion: the central galaxy in an isolated pair has no difference with an isolated galaxy. We discuss the discrepancies with other studies when considering the effects of the galaxy pair in Sect. 4.2.1.

However, we observe significant differences for higher stellar mass bins ($M_\star > 10^{11.0} M_\odot$). This effect is in agreement with Melnyk et al. (2015), which claim that the environmental influence is notable in the highest mass galaxies. For massive galaxies, the fraction of optical AGN in the SIG and SIP samples is slightly higher than in control samples. In particular, the fraction of optical AGN for massive isolated galaxies is higher than in any other sample, in discrepancy with Melnyk et al. (2015), where the fraction of AGN in pairs is only a little higher than in isolated galaxies.

According to the redshift distribution of the samples (lower panel of Fig. 1), we consider that the trends observed in the fraction of AGN subtypes (see lower panels in Fig. 3) are real. Otherwise the trends would be roughly constant in case that a high fraction of low luminosity AGN at low redshift were misclassified as LINERs. These observed trends suggest that low-mass AGNs are dominated by TOs, while high-mass AGNs are dominated by LINERs.

SBA13 interpreted the time sequence from interaction inducing star formation to passive galaxies (Li et al. 2008; Wild et al. 2010) in order from TO, then Seyfert, and then LINER. Even if our statistic for Seyfert-like galaxies is small, we can interpret our result in light of this sequence. According to our results, the transition from TO to LINER is slower in isolated pairs. Unfortunately we do not have a statistically meaningful number of SIP pairs ($N_T = 191, 44, 152$ LINERs, Seyferts, and TOs, respectively) to explore this result as a function of the Q_{pair} .

These results suggest that the black holes of massive ($M_\star > 10^{11.0} M_\odot$) isolated galaxies are still growing while similar mass isolated pairs, SDSS pairs, and SDSS single galaxies have quenched their activity. This value is similar to the transition mass between hot and cold modes of gas accretion in simulations by Kereš et al. (2009). We can therefore conclude that cold gas accretion by secular evolution is sufficient to explain the optical nuclear activity for more massive galaxies. As suggested by SBA13, the decrease of the prevalence of optical AGN and LINER for massive galaxies in denser environments can be explained by the stripping of cold gas and its warming.

4.1.2. Radio AGN

In the exploration of the possible sources of gas fuelling radio AGN and its connection to the environment, it is crucial to discriminate between the different radio AGN modes (Croton et al. 2006; Hardcastle et al. 2007; Tasse et al. 2008). In fact, SBA13 found opposite trends in HERG and LERG radio AGNs with respect to the local density, when LERGs show a clear increase with density. As it is explained in Sect. 2.3, in this study we focus on LERG radio AGNs. It is important to note that the nature of radio AGN is also sensitive to redshift evolution (Karouzos et al. 2014; Cowley et al. 2016; Magliocchetti et al. 2016). Since the galaxies with SBA13 classification are restricted to the narrow redshift range $0.03 \leq z \leq 0.08$ and the samples follow a similar redshift distribution, we do not expect a bias in our comparison caused by the possible redshift evolution.

Generally, radio nuclear activity is strongly related to the stellar mass and the density of galaxies (SBA13). Hence, we do not expect to find a high fraction of radio AGN in low density clusters. This dependence with the galaxy density (large-

scale environment) is even observed in isolated galaxies. Sabater et al. (2008, 2012) do not find any high luminosity radio AGN in isolated galaxies in the AMIGA (Analysis of the interstellar Medium of Isolated GALaxies, Verdes-Montenegro et al. 2005) sample. In fact, the fraction of radio AGN in isolated galaxies is smaller than expected for galaxies with same stellar mass.

A recent study of radio nuclear activity for local galaxies (Kaviraj et al. 2015) discarded AGN to be triggered by internal mass loss (secular processes). In relation to the large-scale environment, they also dismissed that radio AGN are fuelled by cluster-scale cooling flows since their radio detections preferentially lie outside clusters. They therefore conclude that the most important trigger for ‘cold-mode’ radio AGN is galaxy merging. In this regard, Ramos Almeida et al. (2012) and Chiaberge et al. (2015) found strong evidence that mergers are the triggering mechanism for the radio-loud AGN phenomenon. Note that the radio-loud AGNs studied are distinct from the LERGs.

The fraction of radio AGN for single galaxies ($N_T = 33$) and galaxies in pairs ($N_T = 45$) in our study is shown in Fig. 4. The dependence of radio AGN with stellar mass is so strong that, even if the number of radio AGN detections in our samples is small, we can see significant differences with the addition of one single companion. These differences reflect that not only the LSS affects the radio AGN activity, we also found evidence that radio AGN is affected by the local environment. This result is in agreement with Pace & Salim (2014), whose find that radio AGN (LERGs) tend to be located in dense environments. They also claim that they are fuelled by the accretion of small quantities of hot halo gas. Therefore, while the effect of interactions is minimal in triggering optical AGN activity, it seems to have a strong connection with radio AGN activity. Unfortunately, we do not have a statistically significant sample to further explore the dependence on the local and large-scale environments as for optical AGN in this study.

Note here that the differences between the two samples could be reduced if we consider halo masses instead of stellar masses. In fact, Ellison et al. (2015) found that radio AGN (LERGs) are not fuelled by mergers, since they do not find an excess on the fraction of radio AGN (LERGs) when matching control samples in halo mass or D4000. Moreover, the results of Fig. 4 agree with the results of Ellison et al. (2015), whose find an excess of LERGs in pairs if only stellar-mass and redshift are matched.

4.2. Dependence on the environment

There has been some disagreement in the literature regarding the connection between environment and nuclear activity. In this context, we explore the effect of local and large-scale environments on the AGN activity in isolated galaxies and physically bound isolated pairs, selected under a three-dimensional isolation definition. To investigate this, we computed the tidal strengths Q_{pair} and Q_{LSS} as explained in Sect. 2. The different nature of the different environment definitions for isolated systems and the control samples are shown in Fig. 2. By definition, control samples dominate the range of higher values of the Q_{LSS} , while the systems of galaxies in pairs lie in the area of higher Q_{pair} .

4.2.1. Dependence on the local environment

The values of Q_{pair} for SDSS pairs are mainly larger than the values for SIP galaxies, as it is shown in Fig. 2. This is expected since there are more SDSS pairs at smaller projected distances

and higher mass ratio than in isolated pairs. Nevertheless, there is an area with common values of the Q_{pair} between -2.5 to -0.5 (see Fig. 5). We do not observe relevant differences in this common area. In general, we do not observe any significant trend as a function of Q_{pair} (see Fig. 5), neither as a function of ΔQ , which is defined as $Q_{\text{pair}} - Q_{\text{LSS}}$ and quantifies the extent that a given galaxy is dominated by its closest neighbour or its large-scale environment.

On the contrary, Ellison et al. (2011) found an increase in the AGN fraction in most tight pairs and stated that optical AGN might be triggered by close interactions. A possible explanation for the discrepancy is the fairly wide projected separations of the SDSS pairs sample ($d \approx 200$ kpc on average) in comparison to the AGN excess seen in Ellison et al. (2011) at distances $d \lesssim 50$ kpc. To check this we further explore the fraction of optical AGN as a function of the projected separation and the mass ratio between the two galaxies in pairs. Even if we do not have a large statistical sample of isolated pairs with projected separation smaller than 50 kpc ($N_T = 50$), we have a large number ($N_T = 435$) of close SDSS pairs to compare with the results of Ellison et al. (2011). We also do not observe any trend and any relevant difference between the SIP or the SDSS pairs samples with projected separation. This discrepancy might then come from the different definitions of the local environment. For the purpose of the present study, galaxy pairs are located in low density environments. By definition, the SIP sample is very well isolated from the large-scale environment, with the first nearest neighbour at projected distances larger than 1 Mpc. In the case of SDSS pairs, we selected groups in Yang et al. (2007) with two galaxies within the same dark matter halo to avoid the case where the same central galaxy can be included in two or three different pairs. We therefore confirm our previous result that local environment has not a principal role in triggering optical AGN.

The parameters described in Eqs. 1 and 2 quantify the tidal effects onto the central (brightest) galaxy in galaxy pairs. In this sense, high values of these parameters, in relation to the AGN fraction, are mainly associated with the gas stripping or the shape distortion of the central galaxy. Nevertheless, AGN properties are more associated with the gas accretion of the central galaxy. In this sense, an alternative definition of the Q_{pair} , i.e. $Q_{\text{pair,B}} \equiv \log\left(\frac{M_A}{M_B} \left(\frac{D_B}{d_{AB}}\right)^3\right)$, is more closely related to trigger the gas accretion to the central galaxy. To better identify the different contributions it is worth to further explore the tidal strength affecting the faintest galaxy in the galaxy pairs. However, this should be carried out in a separated study since only 45% of the SIP has SBA13 classification for the two members in the mass range considered in the present study (the typical mass ratio is $\sim 1/100$ Argudo-Fernández et al. 2015b).

4.2.2. Dependence on the LSS environment

In contrast to SDSS single galaxies, we find a strong dependence of the LSS on the optical nuclear activity and star formation in isolated galaxies. Moreover, the observed trends are different depending on galaxy mass (see Fig. 6).

According to Argudo-Fernández et al. (2015b), SIG galaxies mainly belong to the outer parts of filaments, walls, and clusters, and generally differ from the void population of galaxies. In fact, only one third of SIG galaxies are located in voids. Using the code for data visualisation LSSGALPY⁷ (Argudo-Fernández et al. 2015a), we checked that galaxies with low values of Q_{LSS}

⁷ <https://github.com/margudo/LSSGALPY>

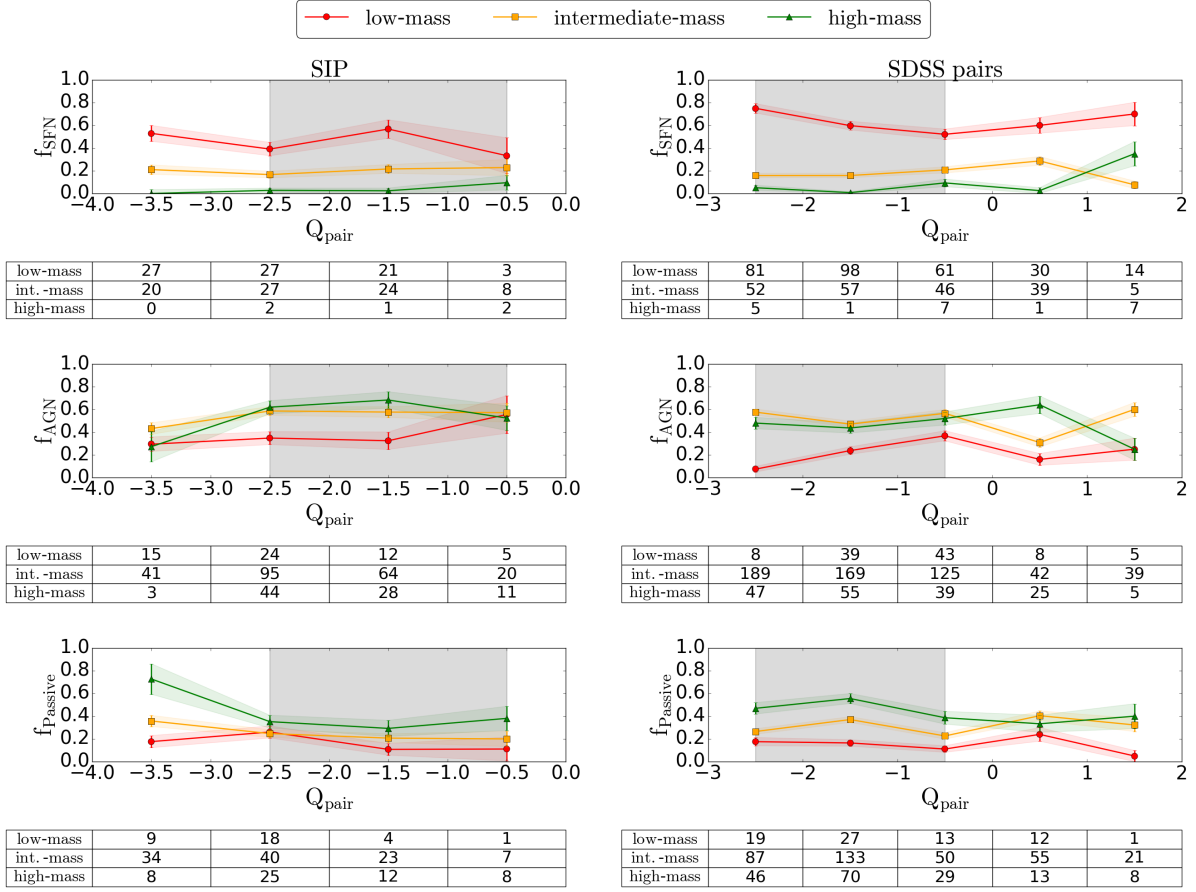


Fig. 5. Fraction of optical nuclear activity with respect to the Q_{pair} environmental parameter. Low-mass galaxies ($10.0 \leq \log(M_{\star}) < 10.5$ [M_{\odot}]) are represented by red circles, intermediate-mass galaxies ($10.5 \leq \log(M_{\star}) < 11.0$ [M_{\odot}]) are represented by orange squares, and high-mass galaxies ($11.0 \leq \log(M_{\star}) \leq 11.4$ [M_{\odot}]) are represented by green triangles. The fraction of SFN, optical AGN, and passive SIP galaxies ($N_T = 169, 387$, and 208 , respectively) is represented from top to bottom in the left panels, and for SDSS pairs ($N_T = 564, 1009$, and 678 , respectively) in the right panels. The number of galaxies in each Q_{pair} bin is shown in tables for each sample at the bottom of each panel. The dashed area in the figures corresponds to the range with common values of Q_{pair} between the two samples, from -2.5 to -0.5 . Error bars are given considering binomial distribution.

are mainly located in void regions, and galaxies with higher Q_{LSS} are more related with denser structures, as filaments or walls. See Appendix A for more details.

This means that the differences that we found between SIG galaxies and SDSS singles, with respect to high values of the Q_{LSS} , are directly related to the location of the galaxies in the outskirts or inside clusters, respectively. According to this, the general trend for the fraction of passive isolated galaxies is to decrease from voids to denser regions (e. g. clusters, filaments). However, the fraction is smaller than that of similar mass SDSS single galaxies located in the same regions.

The fraction of optical AGN for high-mass SIG galaxies increases with denser large-scale environment (massive SIG galaxies have more accretion time and therefore they have more gas). We interpret this result as the central black hole in massive isolated galaxies being fuelled by cold gas from the LSS. We would not see an increment in SDSS single galaxies because of the warming of the cold gas in denser environments, where the effect of the stripping of diffuse gas or strangulation, ram-pressure stripping, and galaxy harassment is present. (von der Linden et al. 2010; Peng et al. 2015).

On the contrary, the fraction of optical AGN for low-mass SIG galaxies decreases from voids to denser regions (e.g. clusters, filaments). In comparison to the trend for passive galaxies,

this is directly translated into an important increment of star-forming SIG galaxies in the outskirts of clusters. Given that the fraction of star-forming SIG galaxies with low values of Q_{LSS} is smaller, our results contrast to those of Liu et al. (2015). They found that the fraction of star-forming galaxies in voids is significantly higher than that in walls. Note that only 14% of void galaxies in Pan et al. (2012) are found in the SIG sample (Argudo-Fernández et al. 2015b), therefore void galaxies span a large range of local environments. In the future, we will explore these differences further by considering the possible effect of morphology or stellar populations.

We previously discussed the fact that the fraction of optical AGN in the SIG sample continues increasing, while peaks at $M_{\star} \approx 10^{8.0} M_{\odot}$ for the other samples (see Fig. 3). From Fig. 6, we see that this continue increase mainly occurs at high Q_{LSS} . It is interesting that, on the contrary, the AGN fraction of the low-mass SIG galaxies even decreases. Such a different mass dependent worth a further detailed study.

The different mass- and environment-dependence behaviours between isolated and control samples suggest that a halo/mass or a simple Q_{LSS} parameter is not enough to characterise the environmental effects of galaxies in more complicated (small-scale) environments.

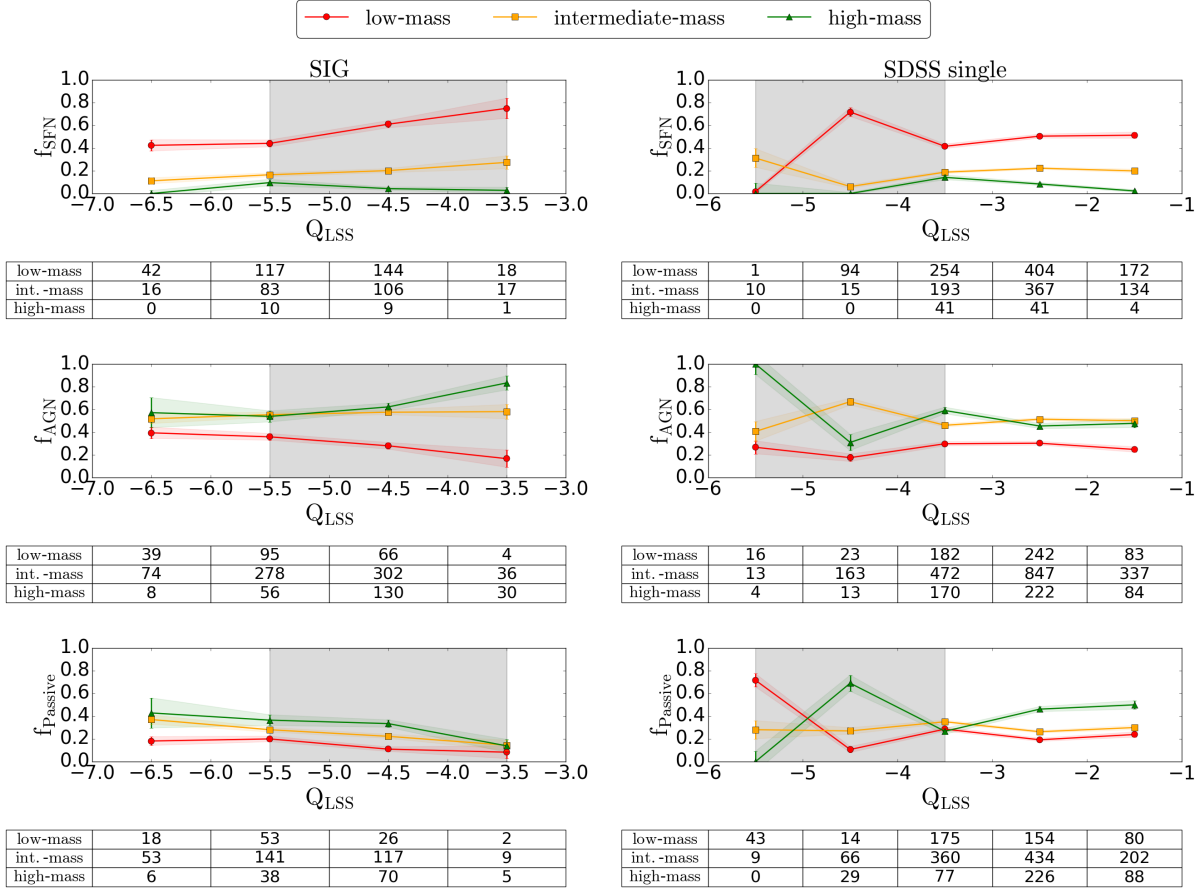


Fig. 6. Fraction of optical nuclear activity with respect to the Q_{LSS} environmental parameter. Low-mass galaxies ($10.0 \leq \log(M_\star) < 10.5$ [M_\odot]) are represented by red circles, intermediate-mass galaxies ($10.5 \leq \log(M_\star) < 11.0$ [M_\odot]) are represented by orange squares, and high-mass galaxies ($11.0 \leq \log(M_\star) \leq 11.4$ [M_\odot]) are represented by green triangles. The fraction of SFN, optical AGN, and passive SIG galaxies ($N_r = 587, 1153$, and 559 , respectively) is represented from top to bottom in the left panels, and for SDSS single galaxies ($N_r = 1777, 3027$, and 2063 , respectively) in the right panels. The number of galaxies in each Q_{LSS} bin is shown in tables for each sample at the bottom of each panel. The dashed area in the figures corresponds to the range with common values of Q_{LSS} between the two samples, from -5.5 to -3.5 . Error bars are given considering binomial distribution.

5. Summary and conclusions

In this work we study the effect of the environment on the fraction of optical and radio nuclear activity. In particular, we investigate the effect of both, local and large-scale environments on nuclear activity and star formation, for the first time using three-dimensional isolated galaxies and physically bound isolated pairs (SIG and SIP galaxies, respectively). Besides, using the tidal strength parameters Q_{pair} and Q_{LSS} we are able to quantify separately the effect of one-on-one interactions from the effect of the large-scale environment where the galaxy resides. Control samples of single galaxies and pairs selected from the SDSS were used for comparison.

Our main conclusions are the following:

1. The prevalence of optical AGN is found to be independent to the addition of one single companion (see Fig. 3).
2. For massive galaxies, the fraction of optical AGN in isolated galaxies and isolated pairs is slightly higher than in the control samples (see the central upper panel in Fig. 3). Moreover, the fraction of massive passive isolated galaxies is smaller than in any other sample (see the right upper panel in Fig. 3). These results suggest that the black holes of massive ($\log(M_\star) > 11.0$ [M_\odot]) isolated galaxies are still grow-

ing while similar mass isolated pairs, SDSS pairs, and SDSS single galaxies have already quenched their activity.

3. Local environment has not a principal role in triggering optical AGN (see Fig. 5). Cold gas accretion by secular evolution is sufficient to explain the optical nuclear activity for more massive galaxies (see the middle left panel in Fig. 6).
4. In contrast to local environment, we find a strong dependence of the optical nuclear activity and star formation on the LSS for isolated systems (see Fig. 6). In particular, the fraction of AGN for high-mass SIG galaxies increases with denser large-scale environment. We interpret this result as the central black hole in massive isolated galaxies being fuelled by cold gas from the LSS.
5. Regarding to radio nuclear activity (LERG), we find that not only the galaxy mass and large-scale environment affects it, but that radio AGN are also strongly affected by the local environment (see Fig. 4).

Optical AGN is related to cold gas accretion, while radio AGN is related to hot gas accretion. In this context, there is more cold gas, fuelling the central optical AGN, in isolated systems. Overall, our results are in agreement with a scenario where cold gas accretion by secular evolution is the main driver for optical AGN, while hot gas accretion and one-on-one interactions are the main drivers of radio AGN activity.

Acknowledgments

The authors acknowledge the anonymous referee for his/her very detailed and useful report, which helped to clarify and improve the quality of this work.

MAF is grateful for financial support from PIFI (funded by Chinese Academy of Sciences President's International Fellowship Initiative) Grant No. 2015PM056 and from CONICYT FONDECYT project No. 3160304. This work was partly supported by the Strategic Priority Research Program "The Emergence of Cosmological Structures" of the Chinese Academy of Sciences (CAS; grant XDB09030200), the National Natural Science Foundation of China (NSFC) with the Project Number of 11573050 and 11433003, and the "973 Program" 2014 CB845705. This work was partially supported by Ministerio de Economía y Competitividad and by FEDER (Fondo Europeo de Desarrollo Regional) via grants AYA2011-24728, AYA2013-47742-C04-01, AYA2014-53506-P, and from the "Junta de Andalucía" local government through the FQM-108 project.

This research made use of *ASTROPY*, a community-developed core *PYTHON* (<http://www.python.org>) package for Astronomy (*Astropy Collaboration et al. 2013*); *IPYTHON* (*Pérez & Granger 2007*); *MATPLOTLIB* (*Hunter 2007*); *NUMPY* (*Walt et al. 2011*); *SCIPY* (*Jones et al. 2001*); and *TOPCAT* (*Taylor 2005*).

Funding for SDSS-III has been provided by the Alfred P. Sloan Foundation, the Participating Institutions, the National Science Foundation, and the U.S. Department of Energy Office of Science. The SDSS-III web site is <http://www.sdss3.org/>.

References

- Abazajian, K. N., Adelman-McCarthy, J. K., Agüeros, M. A., et al. 2009, *ApJS*, 182, 543
- Abell, G. O. 1958, *ApJS*, 3, 211
- Ahn, C. P., Alexandroff, R., Allende Prieto, C., et al. 2014, *ApJS*, 211, 17
- Alam, S., Albareti, F. D., Allende Prieto, C., et al. 2015, *ApJS*, 219, 12
- Alexander, D. M. & Hickox, R. C. 2012, *New A Rev.*, 56, 93
- Argudo-Fernández, M., Duarte Puertas, S., Verley, S., Sabater, J., & Ruiz, J. E. 2015a, *LSSGALPY: Visualization of the large-scale environment around galaxies on the 3D space*, *Astrophysics Source Code Library*, record ascl:1505.012
- Argudo-Fernández, M., Verley, S., Bergond, G., et al. 2015b, *A&A*, 578, A110
- Argudo-Fernández, M., Verley, S., Bergond, G., et al. 2014, *A&A*, 564, A94
- Argudo-Fernández, M., Verley, S., Bergond, G., et al. 2013, *A&A*, 560, A9
- Astropy Collaboration*, Robitaille, T. P., Tollerud, E. J., et al. 2013, *A&A*, 558, A33
- Baldry, I. K., Glazebrook, K., Brinkmann, J., et al. 2004, *ApJ*, 600, 681
- Baldwin, J. A., Phillips, M. M., & Terlevich, R. 1981, *PASP*, 93, 5
- Becker, R. H., White, R. L., & Helfand, D. J. 1995, *ApJ*, 450, 559
- Bell, E. F., McIntosh, D. H., Katz, N., & Weinberg, M. D. 2003, *ApJS*, 149, 289
- Best, P. N. & Heckman, T. M. 2012, *MNRAS*, 421, 1569
- Best, P. N., Kauffmann, G., Heckman, T. M., et al. 2005a, *MNRAS*, 362, 25
- Best, P. N., Kauffmann, G., Heckman, T. M., & Ivezić, Ž. 2005b, *MNRAS*, 362, 9
- Blanton, M. R. & Roweis, S. 2007, *AJ*, 133, 734
- Blanton, M. R., Schlegel, D. J., Strauss, M. A., et al. 2005, *AJ*, 129, 2562
- Boselli, A. & Gavazzi, G. 2014, *A&A Rev.*, 22, 74
- Brinchmann, J., Charlot, S., White, S. D. M., et al. 2004, *MNRAS*, 351, 1151
- Calvi, R., Poggianti, B. M., Fasano, G., & Vulcani, B. 2012, *MNRAS*, 419, L14
- Casado, J., Ascasibar, Y., Gavilán, M., et al. 2015, *MNRAS*, 451, 888
- Chiaberge, M., Gilli, R., Lotz, J. M., & Norman, C. 2015, *ApJ*, 806, 147
- Choi, Y.-Y., Woo, J.-H., & Park, C. 2009, *ApJ*, 699, 1679
- Condon, J. J., Cotton, W. D., Greisen, E. W., et al. 1998, *AJ*, 115, 1693
- Cowley, M. J., Spitler, L. R., Tran, K.-V. H., et al. 2016, *MNRAS*, 457, 629
- Coziol, R., Torres-Papaqui, J. P., Plauchu-Frayn, I., et al. 2011, *Rev. Mexicana Astron. Astrofis.*, 47, 361
- Croton, D. J., Springel, V., White, S. D. M., et al. 2006, *MNRAS*, 365, 11
- Dressler, A. 1980, *ApJ*, 236, 351
- Ellison, S. L., Patton, D. R., & Hickox, R. C. 2015, *MNRAS*, 451, L35
- Ellison, S. L., Patton, D. R., Mendel, J. T., & Scudder, J. M. 2011, *MNRAS*, 418, 2043
- Fabian, A. C. 1999, *MNRAS*, 308, L39
- Grützbauch, R., Conselice, C. J., Varela, J., et al. 2011, *MNRAS*, 411, 929
- Hardcastle, M. J., Evans, D. A., & Croston, J. H. 2007, *MNRAS*, 376, 1849
- Heckman, T. M. 1980, *A&A*, 87, 152
- Hernández-Ibarra, F. J., Dultzin, D., Krongold, Y., et al. 2013, *MNRAS*, 434, 336
- Hernández-Ibarra, F. J., Krongold, Y., Dultzin, D., et al. 2016, *MNRAS*[arXiv:1509.02186]
- Hine, R. G. & Longair, M. S. 1979, *MNRAS*, 188, 111
- Hong, J., Im, M., Kim, M., & Ho, L. C. 2015, *ApJ*, 804, 34
- Hunter, J. D. 2007, *Computing In Science & Engineering*, 9, 90
- Jones, E., Oliphant, T., Peterson, P., et al. 2001, *SciPy: Open source scientific tools for Python*, [Online; accessed 2016-01-15]
- Karouzos, M., Im, M., Kim, J.-W., et al. 2014, *ApJ*, 797, 26
- Kauffmann, G., Heckman, T. M., Tremonti, C., et al. 2003a, *MNRAS*, 346, 1055
- Kauffmann, G., Heckman, T. M., White, S. D. M., et al. 2003b, *MNRAS*, 341, 33
- Kauffmann, G., White, S. D. M., Heckman, T. M., et al. 2004, *MNRAS*, 353, 713
- Kaviraj, S., Shabala, S. S., Deller, A. T., & Middelberg, E. 2015, *MNRAS*, 452, 774
- Kereš, D., Katz, N., Fardal, M., Davé, R., & Weinberg, D. H. 2009, *MNRAS*, 395, 160
- Li, C., Kauffmann, G., Heckman, T. M., White, S. D. M., & Jing, Y. P. 2008, *MNRAS*, 385, 1915
- Liu, C.-X., Pan, D. C., Hao, L., et al. 2015, *ApJ*, 810, 165
- Lynden-Bell, D. 1969, *Nature*, 223, 690
- Magliocchetti, M., Lutz, D., Santini, P., et al. 2016, *MNRAS*, 456, 431
- Manzer, L. H. & De Robertis, M. M. 2014, *ApJ*, 788, 140
- McAlpine, K., Prandoni, I., Jarvis, M., et al. 2015, *Advancing Astrophysics with the Square Kilometre Array (AASKA14)*, 83
- Melnyk, O., Karachentseva, V., & Karachentsev, I. 2015, *MNRAS*, 451, 1482
- Pace, C. & Salim, S. 2014, *ApJ*, 785, 66
- Pan, D. C., Vogeley, M. S., Hoyle, F., Choi, Y.-Y., & Park, C. 2012, *MNRAS*, 421, 926
- Peng, Y., Maiolino, R., & Cochrane, R. 2015, *Nature*, 521, 192
- Peng, Y.-j., Lilly, S. J., Kovač, K., et al. 2010, *ApJ*, 721, 193
- Peng, Y.-j., Lilly, S. J., Renzini, A., & Carollo, M. 2012, *ApJ*, 757, 4
- Pérez, F. & Granger, B. E. 2007, *Computing in Science and Engineering*, 9, 21
- Pulatova, N. G., Vavilova, I. B., Sawangwit, U., Babyk, I., & Klimanov, S. 2015, *MNRAS*, 447, 2209
- Ramos Almeida, C., Bessiere, P. S., Tadhunter, C. N., et al. 2012, *MNRAS*, 419, 687
- Rosario, D. J., Mendel, J. T., Ellison, S. L., Lutz, D., & Trump, J. R. 2016, *MNRAS*, 457, 2703
- Sabater, J., Best, P. N., & Argudo-Fernández, M. 2013, *MNRAS*, 430, 638
- Sabater, J., Best, P. N., & Heckman, T. M. 2015, *MNRAS*, 447, 110
- Sabater, J., Leon, S., Verdes-Montenegro, L., et al. 2008, *A&A*, 486, 73
- Sabater, J., Verdes-Montenegro, L., Leon, S., Best, P., & Sulentic, J. 2012, *A&A*, 545, A15
- Salim, S., Rich, R. M., Charlot, S., et al. 2007, *ApJS*, 173, 267
- Salpeter, E. E. 1964, *ApJ*, 140, 796
- Satyapal, S., Ellison, S. L., McAlpine, W., et al. 2014, *MNRAS*, 441, 1297
- Shakura, N. I. & Sunyaev, R. A. 1973, *A&A*, 24, 337
- Shen, S.-Y., Argudo-Fernández, M., Chen, L., et al. 2016, *Research in Astronomy and Astrophysics*, 16, 007
- Soltan, A. 1982, *MNRAS*, 200, 115
- Strauss, M. A., Weinberg, D. H., Lupton, R. H., et al. 2002, *AJ*, 124, 1810
- Tasse, C., Best, P. N., Röttgering, H., & Le Borgne, D. 2008, *A&A*, 490, 893
- Taylor, M. B. 2005, in *Astronomical Society of the Pacific Conference Series*, Vol. 347, *Astronomical Data Analysis Software and Systems XIV*, ed. P. Shopbell, M. Britton, & R. Ebert, 29
- Tremonti, C. A., Heckman, T. M., Kauffmann, G., et al. 2004, *ApJ*, 613, 898
- Verdes-Montenegro, L., Sulentic, J., Lisenfeld, U., et al. 2005, *A&A*, 436, 443
- Verley, S., Leon, S., Verdes-Montenegro, L., et al. 2007, *A&A*, 472, 121
- von der Linden, A., Wild, V., Kauffmann, G., White, S. D. M., & Weinmann, S. 2010, *MNRAS*, 404, 1231
- Walt, S. v. d., Colbert, S. C., & Varoquaux, G. 2011, *Computing in Science & Engineering*, 13, 22
- Wild, V., Heckman, T., & Charlot, S. 2010, *MNRAS*, 405, 933
- Yang, X., Mo, H. J., van den Bosch, F. C., et al. 2007, *ApJ*, 671, 153
- York, D. G., Adelman, J., Anderson, J. J. E., et al. 2000, *AJ*, 120, 1579
- Zhao, G., Zhao, Y.-H., Chu, Y.-Q., Jing, Y.-P., & Deng, L.-C. 2012, *Research in Astronomy and Astrophysics*, 12, 723

Appendix A: LSSGALPY

LSSGALPY⁸ (Argudo-Fernández et al. 2015a) is a tool for the interactive visualization of the large-scale environment around galaxies on the 3D space based on Python language. The tool allows one to easily compare the 3D positions of a sample (or samples) with respect to the locations of the LSS galaxies in their local and/or large scale environments. For the purpose of this study, we compared the position of galaxies in the SIG sample according to three different ranges of values of their Q_{LSS} (see a snapshot of the tool in Fig. A.1).

We observe that most of the SIG galaxies with $Q_{\text{LSS}} \leq -5.5$ are preferentially located in voids or low density regions, while SIG galaxies with $-5.5 < Q_{\text{LSS}} \leq -4.5$, and specially with $Q_{\text{LSS}} > -4.5$, are distributed along the LSS. This means that these SIG galaxies mainly belong to the outer parts of filaments, walls, and clusters, and generally differ from the void population of galaxies.

⁸ Available at <https://github.com/margudo/LSSGALPY>

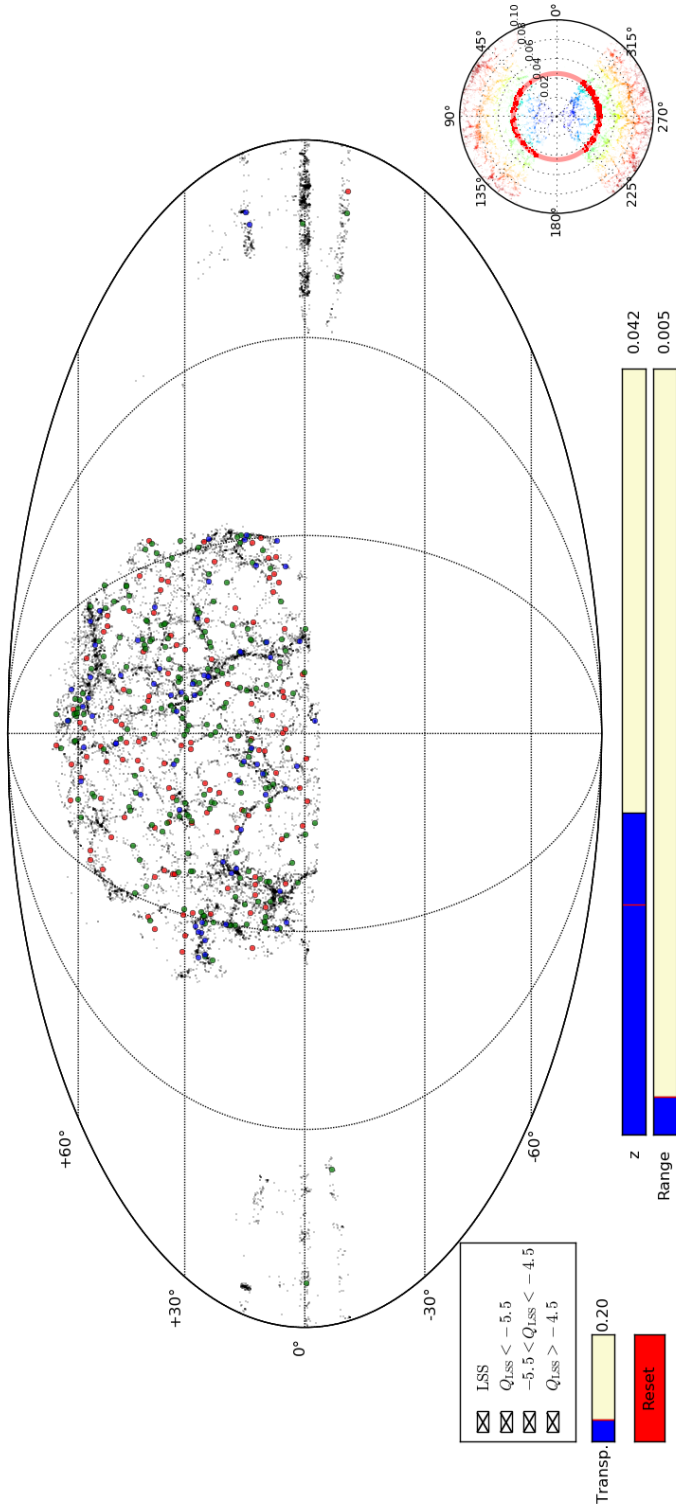
Mollweide projection within $0.042 < z < 0.047$


Fig. A.1. Interactive 3D visualisation software: Mollweide projection. Mollweide projection of the LSS for galaxies (black points) in the redshift range $0.042 < z < 0.047$ as shown in the blue bars in the lower part of the figure. Red disks represent SIG galaxies with $Q_{LSS} \leq -5.5$ within the same redshift range. Green disks represent SIG galaxies with $-5.5 < Q_{LSS} \leq -4.5$ within the same redshift range. Blue disks represent SIG galaxies with $Q_{LSS} > -4.5$ within the same redshift range. To guide the eye, a wedge diagram, for LSS galaxies within -2 and 2 degrees in declination, is shown in the right lower part of the figure. Colour code according to the redshift from $z = 0$ (blue) to $z = 0.10$ (red). The red ring in the polar representation corresponds to the selected redshift range in the central Mollweide projection.